

# Acceleration of Cosmic Rays in Supernova Shocks: elemental selectivity of the injection mechanism

A. Hanusch\* and T. Liseykina

*Institut für Physik, Universität Rostock, 18051 Rostock, Germany*

M. Malkov

*CASS and Department of Physics, University of California, San Diego, La Jolla, California 92093, USA*

(Dated: March 13, 2022)

Precise measurements of galactic cosmic rays test mechanisms of their selective acceleration in supernova shocks. According to one mechanism, the mass-to-charge ratio  $A/Z$  is the key to selection. Striking similarities between He/ $p$ , C/ $p$ , and O/ $p$  rigidity spectra, recently measured by AMS-02, confirms the premise. We study this mechanism by simulating a collisionless shock. A selection rate  $\eta$  increases with  $A/Z$ , saturates, and peaks as a function of Mach number  $M$ . The dependence  $\eta(M, A/Z)$  obtained from simulations and convoluted with the shock time dependence through  $M(t)$ , accurately reproduces the AMS-02 data.

*Introduction* – The PAMELA experiment [1] accurately determined a  $\approx 0.1$  difference between the rigidity spectral indices of protons and helium. Similar deviations have been indicated earlier by other experiments [2] and confirmed by the recent high-fidelity AMS-02 measurements [3], Fig. 1. According to other observations [4], the scaling shown in Fig. 1 is likely to continue to higher rigidities. These findings call into question the leading hypothesis of cosmic ray (CR) origin, which reads, that the CR particles are accelerated out of an interstellar plasma of the Milky Way when it is swept by blast waves of supernovae.

The CR acceleration mechanism is believed to be electromagnetic in nature. Particles gain energy while being scattered by converging plasma flows upstream and downstream of a supernova remnant (SNR) shock. The mechanism was originally proposed by Fermi [5] and actively researched under the name diffusive shock acceleration (DSA). It is rather easy to show that even a small, e.g., a  $\approx 0.1$ , difference in the rigidity spectral indices of different elements may seriously undermine any (not only the DSA!) electromagnetic acceleration mechanism. In fact, the particle equations of motion written in terms of their rigidity,  $\mathcal{R} = \mathbf{p}c/eZ$ , instead of momentum  $\mathbf{p}$  ( $Z$  is the charge number) read

$$\frac{1}{c} \frac{d\mathcal{R}}{dt} = \mathbf{E}(\mathbf{r}, t) + \frac{\mathcal{R} \times \mathbf{B}(\mathbf{r}, t)}{\sqrt{\mathcal{R}_0^2 + \mathcal{R}^2}}, \quad (1)$$

$$\frac{1}{c} \frac{d\mathbf{r}}{dt} = \frac{\mathcal{R}}{\sqrt{\mathcal{R}_0^2 + \mathcal{R}^2}}. \quad (2)$$

The electric,  $\mathbf{E}(\mathbf{r}, t)$ , and magnetic,  $\mathbf{B}(\mathbf{r}, t)$ , fields here are completely arbitrary. So, the equations apply not only to the acceleration of CRs in a SNR shock but also to their propagation through the turbulent interstellar medium (ISM) to an observer. The propagation

also includes an eventual escape of the accelerated CRs from the Milky Way. It follows that all species with  $\mathcal{R} \gg \mathcal{R}_0 = Am_p c^2 / Ze$  ( $A$  is the atomic number and  $m_p$  the proton mass, so  $\mathcal{R}_0 \propto A/Z$  GV) have nearly identical orbits in the phase space  $(\mathbf{r}, \mathcal{R})$ . If, say, protons and helium ions are already accelerated to  $\mathcal{R} = \mathcal{R}_1 \gg \mathcal{R}_0$  with a stationary  $p/\text{He}$  ratio, this same ratio will persist for all  $\mathcal{R} \gg \mathcal{R}_0$ , in apparent contradiction with Fig. 1.

Three different ideas have been entertained to explain the above paradox: (1) contributions from several SNRs with different  $p/\text{He}$  mixes and spectral slopes; (2) CR spallation in the ISM that introduces particle sources and sinks in Eq. (1); (3) shock evolution in time. Assuming the  $p/\text{He}$  ratio fixed at some fiducial rigidity  $\mathcal{R} = \mathcal{R}_1 \gg \mathcal{R}_0$ , it must increase while the shock strength naturally decreases. While not impossible, the  $p/\text{He}$  increase must occur at a rate consistent with the observed  $p/\text{He}$  slope in rigidity. The crucial point here is that the power-law index of shock-accelerated particles,  $q$ , decreases with the Mach number  $M(t)$  rather definitively:  $q = -d \ln f / d \ln \mathcal{R} = 4 / (1 - M^{-2})$ , where  $f$  is the CR distribution function. Therefore, to reproduce the 0.1 index difference between  $p$  and He correctly, the  $p/\text{He}$  ratio at  $\mathcal{R} = \mathcal{R}_1$  must depend on the shock Mach number in a specific way. This dependence, in turn, is an intrinsic property of collisionless shock and cannot be adjusted to fit the data, thus making the scenario (3) fully testable.

Unlike the scenario (3) above, (1) is not testable because the individual properties of contributing sources are unknown. Besides, it will likely fail the Occam's razor test, especially after the AMS-02 has measured  $p/\text{C}$  and  $p/\text{O}$  ratios to be identical to those of  $p/\text{He}$  [7]. It was also pointed out in [8] that it would be impossible to maintain the spectral slopes in these ratios nearly constant over an extended rigidity range. Meanwhile, according to [9], the spallation effects (2) cannot fully explain the  $p/\text{He}$  rigidity dependence, either. It follows that the time dependence of the subrelativistic acceleration phase (injection into DSA, option (3) above) is the most realistic scenario to consider.

\* Corresponding author: adrian.hanusch@uni-rostock.de

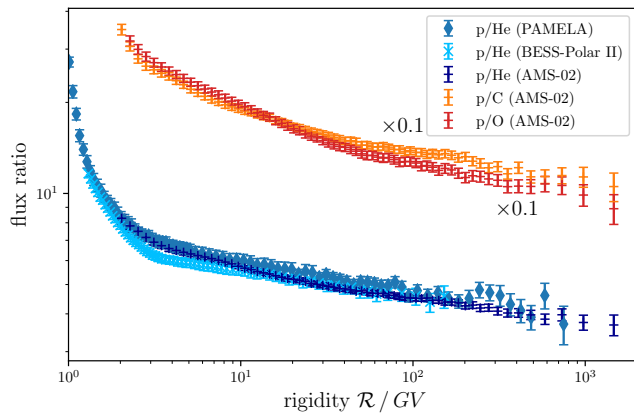


FIG. 1. The  $p/\text{He}$ ,  $p/\text{C}$ , and  $p/\text{O}$  ratio as a function of particle rigidity. The data is taken from [1, 3, 6, 7].

The time dependence of particle acceleration at an SNR shock comes in two flavors. Firstly, the medium into which the shock propagates may be inhomogeneous [10] (effect of SNR environment). If also the background  $p/\text{He}$  ratio increases outward, this ratio will decrease with rigidity after the acceleration, since higher rigidities are dominated by earlier times of acceleration history when the He contribution was higher. Secondly, the shock weakening also makes the acceleration time dependent. The primary problem with the environmental explanation is that not only the He concentration must be *assumed* to decrease with growing shock radius at a specific rate (one free parameter), but also the carbon and oxygen concentrations must decrease at the same rate (two more free parameters). This conclusion follows from the C/He and O/He flux ratios being independent of rigidity [7, 11]. So, He, C, and O are likely to share their acceleration and propagation history. One corollary of this is that C and O are unlikely to be preaccelerated from grains, contrary to some earlier suggestions [12]. Moreover, the equivalence between the He, C and O spectra corroborates the conclusion [9] that spallation effects are insufficient to account for the observed differences in rigidity spectra between  $p$  and elements whose  $A/Z$  values are similar but higher than that of the protons. Note that it is crucial to use the rigidity dependence of the *fractions* of different species as a primary probe into the intrinsic properties of CR accelerators. Unlike the individual spectra, the fractions are unaffected by the CR propagation, reacceleration, and losses from the galaxy, as long as the spallation is negligible.

Besides being in tension with the AMS-02 recent results, the mechanisms considered so far require special conditions, such as how the CR sources are distributed in the ISM, types of supernova progenitors, or their environments. The question is then if a shock can modify an element abundance at higher energies by selectively accelerating it out of a homogeneous background plasma with no additional assumptions? It has been argued in [13] that

such elemental selectivity of the initial phase of the DSA (injection) must, indeed, occur in quasi-parallel shocks. The injection mechanism was shown to have the following properties: it depends on the shock Mach number; its efficiency increases with  $A/Z$ , then saturates at a level that grows with  $M$ . These properties have been established by analytic calculations of ion injection into the DSA [13–15]. The publication of high-precision measurements of  $p/\text{He}$  ratio by the PAMELA collaboration [1], prompted the authors of [16] to apply the analytic injection theory to the case  $A/Z = 2$  (specifically to  $\text{He}^{2+}$ , also valid for fully stripped C and O, accurately measured later by AMS-02), producing an excellent fit to the PAMELA data in the relevant rigidity range  $2 < \mathcal{R} < 200$  GV. Note that lower rigidities are strongly affected by solar modulation, while at higher rigidities the PAMELA statistics was insufficient to make a meaningful comparison.

The purpose of this paper is to demonstrate that the recent high-precision measurements of elemental spectra with different  $A/Z$  are not only consistent with the hypothesis of CR origin in the SNR, but also strongly support it. Although a similar stand has been taken in [16] about the PAMELA findings [1], the new AMS-02 data [7] and recent progress in shock simulations allow us to establish crucial missing links in the CR-SNR relation. In particular, the coincidence in accelerated particle spectral slopes of three different elements with  $A/Z \simeq 2$  (He, C, and O) discovered by the AMS-02 experiment points to an intrinsic,  $A/Z$ -based element selection mechanism and rules out incidental ones, such as particle injection from inhomogeneous shock environments, incompletely ionized upstream media, or preacceleration of elements locked into grains. It is important to emphasize here that the latter mechanism was primarily justified by an integrated abundance of different elements, whereas the detailed rigidity spectra have become known only now. On the theoretical side, the  $p/\text{He}$  calculations in [16] have been based on an analytic theory that allows some freedom in choosing seed particles for injection [14]. These aspects have been recently discussed, along with the limitations of hybrid simulations in [8]. Nevertheless, simulations can remove many uncertainties in the analysis, thus greatly improving our understanding of the  $A/Z$  selectivity.

*Self-regulation and elemental selectivity of injection* – Suprathermal protons (shock-reflected, or “evaporating” [17] from hot downstream plasma) drive unstable Alfvén waves in front of the shock. These waves control the injection of all particles by regulating their access to those parts of the phase space from where they can repeatedly cross the shock, thus gaining more energy. As protons drive these waves, the waves also trap protons most efficiently. Furthermore, the waves are almost frozen into the local fluid so, when crossing the shock interface, they trap most particles and prevent them from escaping upstream *again*, thus significantly reducing their odds for injection. As noted above, most efficient is namely the proton trapping, while, e.g.,  $\text{He}^{2+}$  ions have somewhat

better chances to escape from the proton-generated waves upstream and to get eventually injected. The trapping becomes naturally stronger with growing wave amplitude that also grows with the Mach number. This trend is more pronounced for the protons than He, which is crucial for the injection selectivity.

The analytic treatment described above has another potentially important limitation that we remove using hybrid simulations. Namely, He ions have not been included in the wave generation upstream and treated only as test particles. Several hybrid simulations, addressing the acceleration efficiency of alpha particles, did include them self-consistently [18, 19], however in some cases with reduced abundances, e.g. [20], making them dynamically unimportant. The fully self-consistent simulations, however, do not provide sufficiently detailed Mach number scans of the  $p/\text{He}$  injection ratio, that is needed to test the injection bias mechanism discussed earlier. Although the test particle approximation is often considered to be sufficient because of the large ( $\simeq 10$ )  $p/\text{He}$  number density ratio, the He ions drive resonant waves that are typically two times longer than the waves driven by the protons. In the wave-particle interaction, the resonance condition is often more important than the wave amplitude. In addition, the rational relation between the respective wave lengths (2:1) is suggestive of parametric interactions between them. Such interaction should facilitate a cascade to longer waves which are vital for the DSA, not just for particle injection. To test the theoretically predicted  $p/\text{He}$  injection bias a state-of-the-art self-consistent modeling is required.

*Simulations* – We study the particle injection into the DSA using hybrid simulations, which is justified because the ions determine the relevant scales. The electrons are treated as a massless fluid; the electron pressure  $p_e$  and the resistivity are both assumed to be isotropic, i.e., scalar quantities. The electron pressure is modeled using an adiabatic equation of state, yielding the relation between pressure and density  $p_e \sim n^{\gamma_e}$ , with the adiabatic index  $\gamma_e = 5/3$ . The ions are treated kinetically. Both the fluid equation and the equation of motion of the ions are non-relativistic, as  $|\mathbf{v}| \ll c$  holds during the injection phase. In the simulations, lengths are given in units of  $c/\omega_p$ , with  $\omega_p = \sqrt{4\pi n_0 e^2/m_p}$  being the proton plasma frequency, where  $n_0$  is the upstream density and  $e$  and  $m_p$  are the charge and the mass of the proton, respectively. Time is measured in the units of inverse proton gyrofrequency,  $\omega_c^{-1}$ , with  $\omega_c = e B_0/m_p c$ . Here  $B_0$  is the magnitude of the background magnetic field, and the velocity is normalized to the Alfvén velocity  $v_A = B_0/\sqrt{4\pi n_0 m_p}$ .

We use a realistic composition of the plasma including different ion species (with  $A/Z$  up to 16) with number ratios corresponding to the amount of particles in the interstellar matter. The fraction of ions respective to protons is  $\sim 10\%$  for helium and  $\sim 0.04\%$  for carbon and oxygen. Hence helium ions are dynamically important and cannot be regarded as test particles. The simulations are one-dimensional spatially, but all three

components of the fields and velocity are included. The reduced number of dimensions allows us to increase the particle statistics and reduce the grid spacing resulting in lower noise levels and an accurate characterization of the waves, both being crucial for an adequate description of the downstream thermalization process. It requires a well-developed wave turbulence to ensure strong wave-particle interactions with extended resonance overlapping. These conditions are key to the entropy production, e.g. [21], not easy to meet in simulations. They are arguably more important than, e.g., possible shock rippling effects, not captured by 1D simulations. At the same time these, and other phenomena occurring at the shock ramp cannot be accurately characterized within hybrid simulations anyway as they require a full kinetic treatment [22, 23] (for further recent discussion of the relevant simulation aspects see [8]).

The shock simulation is initiated by sending a supersonic and superalfvénic plasma flow with velocity  $v_0 > c_s \approx v_A$  against a reflecting wall. The shock forms due to the interaction of the emerging counter-propagating streams. The background magnetic field is parallel to the shock normal  $\mathbf{B}_0 = B_0 \mathbf{x}$ . The upstream plasma betas are set to  $\beta_e = \beta_i = 1$ . The simulation box has a length up to  $18000 c/\omega_p$ , depending on the initial velocity  $v_0$ . The grid spacing is  $\Delta x = 0.2 c/\omega_p$  with 100 particles per cell for each species and the time step is chosen to be  $\Delta t = 0.01/(v_0/v_A) \omega_c^{-1}$ .

*A/Z dependence of injection* – In order to investigate the mass-to-charge dependence of injection, we have performed simulations for ion species with  $A/Z$  up to 16. In addition to protons, He, C, and O ions were present in the simulation with charge states  $Z = 1$  and  $Z = 2$ . The phase space plots for selected ion species for the upstream flow velocity equal to  $v_0 = 10 v_A$  are shown in Fig. 2. The shock transition is clearly visible in the center of the plots, where the transition from the cold upstream flow to the hot and turbulent downstream plasma occurs. The width in  $v_x$  in the downstream is almost the same for all ion species, indicating higher temperatures for heavier species. Furthermore, the thermalization occurs further downstream for heavier ions and the shock transition is not as sharp as for protons. The presence of ions with large  $|v_x|$  in the up- and downstream demonstrates that some ions have already gained energy and are able to cross the shock front.

The energy spectra of the particles downstream of the shock transition are obtained using a logarithmic binning procedure. The resulting spectra at  $t = 1500 \omega_c^{-1}$  are shown in Fig. 3a. For clarity, only a few species are selected. The energy spectra of all ion species exhibit two main features: a Maxwellian distribution and a power-law tail. The transition from the Maxwellian to the power-law tail is obscured by a contribution of supra-thermal particles. The spectra of ions with higher  $A$  are shifted to higher energies, as the velocity is randomized during the shock crossing; the downstream temperature is higher for heavier ions. For all species,  $\alpha$ ,

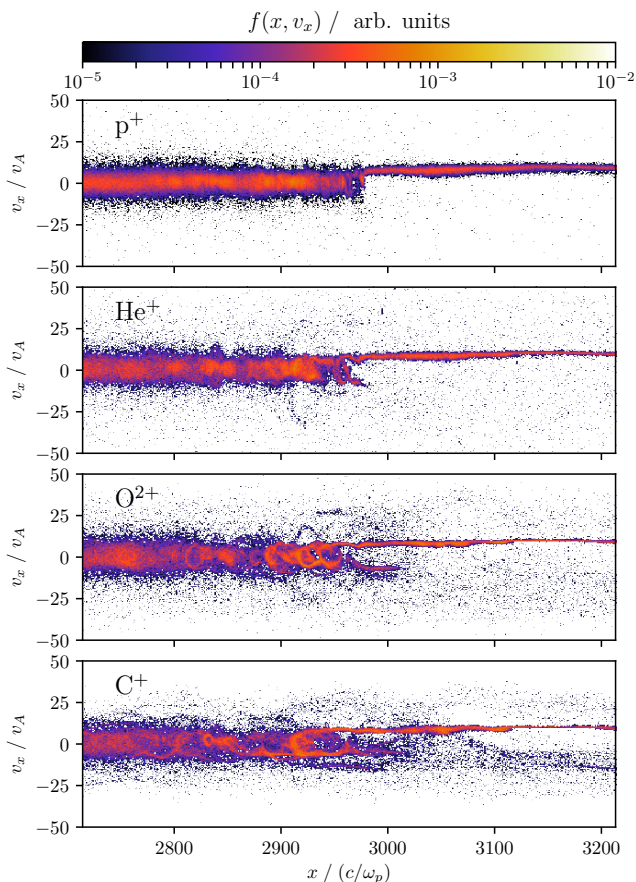


FIG. 2. Phase space  $f(x, v_x)$  for different ion species at  $t = 1000 \omega_c^{-1}$ . The plots show only a part of the simulation domain and are centered around the shock transition. For heavier species thermalization occurs further downstream.

the tail is clearly developed for energies  $E > 10 E_0^\alpha$  with  $E_0^\alpha = \frac{1}{2} m_\alpha v_0^2$ . This energy is marked in the proton energy spectrum in Fig. 3a by the dashed gray line. After the spectra are converged ( $t > 1500 \omega_c^{-1}$  for  $v_0 = 10 v_A$ ), we calculate the number efficiency, *i.e.*, the fraction of particles in the tail of the distribution function. Figure 3b shows the resulting values as function of  $A/Z$ . For low  $A/Z$  the number efficiency grows almost linearly with  $A/Z$ . A saturation occurs around  $A/Z = 8$ , at higher  $A/Z$  the number efficiency decreases. This is to be expected, since in the limit  $A/Z \rightarrow \infty$  neutral particles simply pass the shock and are not subjected to DSA. Note, that the linear behavior of the number efficiency for low  $A/Z$  was found recently in 2D hybrid simulations of quasi-parallel shocks [20] for  $M > 5$ .

*Proton-to-helium ratio* – In the following we investigate the elemental selectivity of the injection mechanism by focusing on the proton-to-helium ratio. To extract this quantity we need to calculate the injection efficiency of  $p$  and  $\text{He}^{2+}$  ions separately. The direct measurement of the injection efficiency is difficult, because the transition from the Maxwellian distribution to the power-law tail

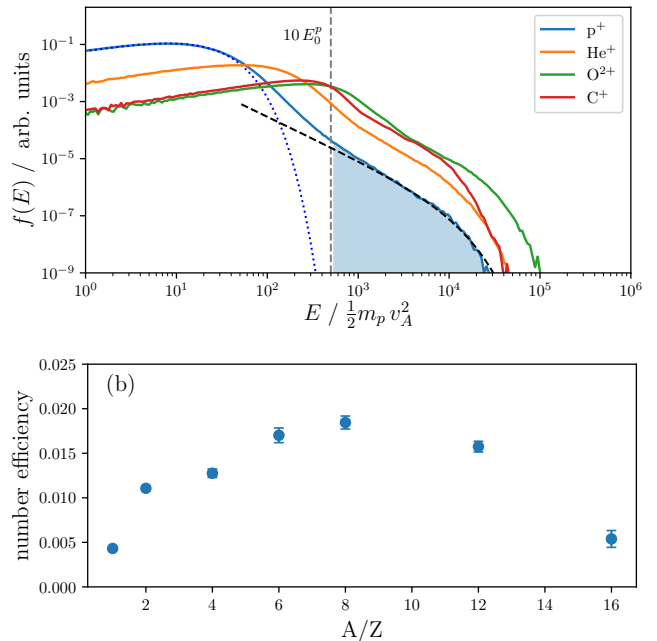


FIG. 3. (a) Downstream energy spectra for some ion species present in the simulation. The protons are assumed to be in the tail of the distribution function if their energy exceeds  $10 E_0^p$  (dashed gray line). The shaded area denotes the part of the spectrum which is used for calculating the number efficiency. (b) Number efficiency as function of the mass-to-charge ratio.

is not sharp. Therefore, we fit a thermal distribution  $f_{\text{th}} = a E^{1/2} \exp(-E/T)$  as well as a power-law with a cut-off,  $f_{\text{pow}} = b E^{-q} \exp(-E/E_{\text{cut}})$  to the low and high energy parts of the downstream spectrum. Here  $T$  is the downstream temperature of the respective ion species and  $E_{\text{cut}}$  is the cut-off energy. The fits are shown for the energy spectrum of protons in Fig. 3a. The dotted cyan line denotes the fitted Maxwellian, and the dashed black line – the power-law fit. The injection efficiency is calculated using the mentioned fits as

$$\eta_{\text{inj}} = \frac{f_{\text{th}}(E_{\text{inj}})}{\int_0^\infty f_{\text{th}}(E) dE} \quad (3)$$

with  $E_{\text{inj}}$  defined from  $f_{\text{th}}(E_{\text{inj}}) = f_{\text{pow}}(E_{\text{inj}})$ .

Figure 4 shows the resulting value of  $\eta_{\text{inj}}^\alpha(M)$  obtained from a series of simulations with different initial upstream flow velocities  $v_0$ , corresponding to different shock Mach numbers,  $M = (v_0 + v_s)/v_A$ . Here  $v_s$  is the shock velocity in the downstream (simulation) rest frame. The injection efficiency as a function of the shock Mach number displays a similar shape for  $p$  and  $\text{He}^{2+}$ . It increases for  $M \lesssim 5$  for  $p$ , and for  $M \lesssim 7$  for  $\text{He}^{2+}$ . For higher  $M$  the injection efficiency decreases for both species. Two aspects are important here. First, the injection of protons dominates for low Mach numbers with  $\eta_{\text{inj}}^p$  exceeding the value of  $\eta_{\text{inj}}^{\text{He}}$  by an order of magnitude. Second, the maximum of  $\eta_{\text{inj}}^p$  is shifted towards smaller  $M$  compared to

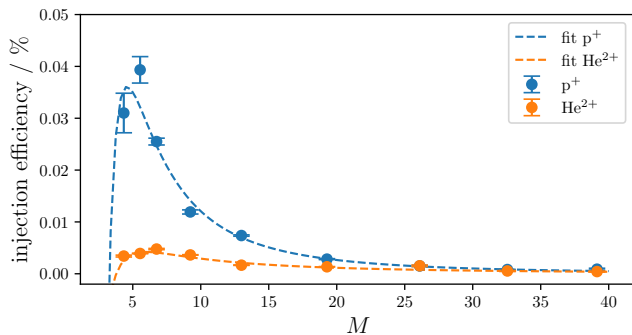


FIG. 4. Injection efficiencies of protons (blue) and helium ions (orange) obtained from the simulation according to Eq. (3) as a function of shock Mach number. The fit parameters are  $a_p = 5.68$ ,  $b_p = 3.27$ ,  $c_p = 3.50$ , and  $a_{\text{He}} = 0.25$ ,  $b_{\text{He}} = 3.79$ ,  $c_{\text{He}} = 2.73$

$\text{He}^{2+}$ . The prevalence of proton injection at slow shocks is also noticeable in the downstream temperature ratio  $T_{\text{He}}/T_p$ , which exceeds for  $M < 15$  the expected ratio of four. At large  $M$  the injection efficiency shows the predicted behavior  $\eta_{\text{inj}}(M) \sim \ln(M/M^*)/M$  (Eq. (76) in [13]).

*Rigidity spectra* – To model the time-dependent CR acceleration we combine the Mach number dependent injection efficiency, Fig. 4, with shock time dependence. It is this combination of injection efficiency obtained from simulations and the theoretical spectral slope,  $q = 4/(1 - M^{-2})$ , which allows us to extend the simulation spectra far beyond in rigidity that any simulation may possibly reach. This extension is justified because our simulation spectra reach the asymptotic DSA power-law regimes, Fig. 3a.

During Sedov-Taylor phase of the SNR evolution the shock radius increases with time as  $R_s \simeq C_{\text{ST}} t^{2/5}$ , while the shock velocity decreases as  $V_s \simeq (2/5) C_{\text{ST}} t^{-3/5} = (2/5) C_{\text{ST}}^{5/2} R_s^{-3/2}$ , with  $C_{\text{ST}} \simeq (2 E_e / \rho_0)^{1/5}$ . Here  $E_e$  is the ejecta energy of the supernova,  $\rho_0$  is the ambient density. The number of CR particles of species  $\alpha$  which are deposited in the shock interior, as the shock radius increases from  $R_{\text{min}}$  to  $R_{\text{max}}$ , can be calculated as

$$N_\alpha(p) \propto \int_{R_{\text{min}}}^{R_{\text{max}}} f_\alpha(p, M(R)) R^2 dR \propto \int_{M_{\text{max}}^{-2}}^{M_{\text{min}}^{-2}} f_\alpha(p, M) dM^{-2}. \quad (4)$$

The spectra here are represented in the following way:

$$f_\alpha \propto \eta_{\text{inj}}^\alpha(M) (\mathcal{R}/\mathcal{R}_{\text{inj}})^{-q(M)} \quad (5)$$

with  $q(M) = 4/(1 - M^{-2})$ .

Instead of feeding the simulation data for  $\eta_{\text{inj}}^\alpha(M)$  directly to the convolution given by Eqs. (4) and (5) we first fit the following simple function  $\eta_{\text{inj}}(M) = a(M-b)M^{-c}$  to the data extracted from the simulations, Fig. 4, and then calculate the proton-to-helium ratio,  $N_p/N_{\text{He}}$ , according to Eq. (4), as a function of rigidity. The results are shown in Fig. 5 by the red line together with the data from the PAMELA and AMS-02 experiments (blue and green shadow areas) and the theoretical fit from [16].

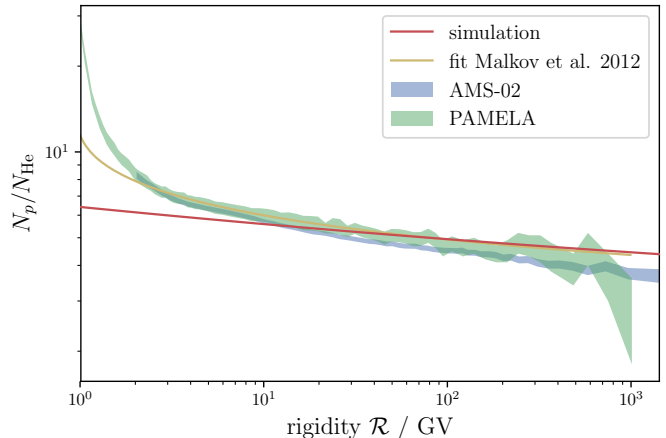


FIG. 5. Proton-to-helium ratio as a function of particle rigidity. The results from the simulation (red line) are compared to the PAMELA and AMS-02 data. For details of the fit (yellow line) see Fig. 3 in [16]. The observed  $p/\text{He}$  ratio is accurately reproduced in the range  $\mathcal{R} \gtrsim 10$ .

*Summary* – Our simulations show that a selection rate of different ion species increases with  $A/Z$ , saturates, and peaks as a function of Mach number  $M$ . They correctly predict the decrease in proton-to-helium ratio with increasing rigidity, Fig. 5, at exactly the rate  $\Delta q \approx 0.1$ , measured in the experiments for  $\mathcal{R} \gtrsim 10$  GV. At lower rigidities,  $\mathcal{R} \lesssim 10$  GV, the difference between the data and our predictions becomes noticeable. Based on the discussion made in the introduction, the difference *must* occur because Eqs. (1), (2) for  $p$  and He deviate towards lower rigidities. Whether the resulting deviation from our prediction based on Eqs. (4) and (5) comes from the accelerator(s), propagation through the ISM or solar modulation, remains unclear. Except for this uncertainty, the suggested mechanism for  $A/Z$ -dependence of the injection fully explains the measured  $p/\text{He}$  ratio.

The research was supported by DFG grant TL2479/2-1, RFBR 16-01-00209, and by NASA ATP-program under grants NNX14AH36G and 80NSSC17K0255. Simulations were performed using the computing resources granted by the North-German Supercomputing Alliance (HLRN) under the project mvp00015.

- 
- [1] O. Adriani *et al.*, *Science* **332**, 69 (2011), <http://science.sciencemag.org/content/332/6025/69.full.pdf>.
- [2] A. D. Panov *et al.*, *Bulletin of the Russian Academy of Sciences: Physics* **73**, 564 (2009).
- [3] M. Aguilar *et al.* (AMS Collaboration), *Phys. Rev. Lett.* **115**, 211101 (2015).
- [4] Y. S. Yoon *et al.*, *The Astrophysical Journal* **728**, 122 (2011).
- [5] E. Fermi, *Phys. Rev.* **75**, 1169 (1949).
- [6] K. Abe *et al.*, *The Astrophysical Journal* **822**, 65 (2016).
- [7] M. Aguilar *et al.* (AMS Collaboration), *Phys. Rev. Lett.* **119**, 251101 (2017).
- [8] M. Malkov, ArXiv e-prints (2017), arXiv:1703.05772 [astro-ph.HE].
- [9] A. E. Vladimirov, G. Jóhannesson, I. V. Moskalenko, and T. A. Porter, *The Astrophysical Journal* **752**, 68 (2012).
- [10] Y. Ohira and K. Ioka, *The Astrophysical Journal Letters* **729**, L13 (2011).
- [11] M. Aguilar *et al.* (AMS Collaboration), *Phys. Rev. Lett.* **120**, 021101 (2018).
- [12] Y. Ohira, N. Kawanaka, and K. Ioka, *Phys. Rev. D* **93**, 083001 (2016).
- [13] M. A. Malkov, *Phys. Rev. E* **58**, 4911 (1998).
- [14] M. A. Malkov and H. J. Völk, *Astronomy and Astrophysics* **300**, 605 (1995).
- [15] M. Malkov and H. Völk, *Advances in Space Research* **21**, 551 (1998), proceedings of the D0.3 Symposium of COSPAR Scientific Commission D which was held during the Thirty-first COSPAR Scientific Assembly.
- [16] M. A. Malkov, P. H. Diamond, and R. Z. Sagdeev, *Phys. Rev. Lett.* **108**, 081104 (2012).
- [17] E. N. Parker, *Journal of Nuclear Energy* **2**, 146 (1961).
- [18] D. Burgess, *Geophysical Research Letters* **16**, 163 (1989).
- [19] K. J. Trattner and M. Scholer, *Geophysical Research Letters* **18**, 1817 (1991).
- [20] D. Caprioli, D. T. Yi, and A. Spitkovsky, *Phys. Rev. Lett.* **119**, 171101 (2017).
- [21] G. M. Zaslavsky, *The physics of chaos in Hamiltonian systems* (world scientific, 2007).
- [22] T. Liseykina, G. Dudnikova, V. Vshivkov, and M. Malkov, *Journal of Plasma Physics* **81** (2015), 10.1017/S002237781500077X.
- [23] M. A. Malkov, R. Z. Sagdeev, G. I. Dudnikova, T. V. Liseykina, P. H. Diamond, K. Papadopoulos, C.-S. Liu, and J. J. Su, *Physics of Plasmas* **23**, 043105 (2016), <https://doi.org/10.1063/1.4945649>.